PALEONTOLOGY

Mesozoic mammaliaforms illuminate the origins of pelage coloration

Ruoshuang Li[1], Liliana D'Alba[2,3], Gerben Debruyn[3], Jessica L. Dobson[3], Chang-Fu Zhou[4,5], Julia A. Clarke[6], Jakob Vinther[7], Quanguo Li[1]*, Matthew D. Shawkey[3]*

Pelage coloration, which serves numerous functions, is crucial to the evolution of behavior, physiology, and habitat preferences of mammals. However, little is known about the coloration of Mesozoic mammaliaforms that coevolved with dinosaurs. In this study, we used a dataset of melanosome (melanin-containing organelle) morphology and quantitatively measured hair colors from 116 extant mammals to reliably reconstruct the coloration of six Mesozoic mammaliaforms, including a previously undescribed euharamiyidan. Unlike the highly diverse melanosomes discovered in feathered dinosaurs, hairs in six mammaliaforms of different lineages and diverse ecomorphotypes showed uniform melanosome geometry, corresponding to dark-brown coloration consistent with crypsis and nocturnality. Our results suggest that the melanosome variation and color expansion seen in extant mammals may have occurred during their rapid radiation and diversification after the Cretaceous-Paleogene extinction.

Integumentary coloration, driven by both sexual and natural selection, is prevalent and serves numerous functions in living organisms, including thermoregulation, crypsis, aposematism, intraspecies recognition, mate selection, and communication (*1*–*5*). Color variability differs between vertebrate clades: Whereas tropical birds exhibit vivid and variable plumage coloration, extant mammals are characterized by relatively subdued shades of black, brown, gray, yellow, or red (*4*). Although limited in their color palette, owing in part to the use of only a single pigment type (melanin) and limited iridescence (*6*, *7*), extant mammals have attained distinctive appearances through the arrangement of those colors in discrete patterns, with adaptive significance recognized since the 19th century (*8*). Despite this importance, as well as long-standing interest from scientists and the public, our understanding of the origin and evolutionary history of mammalian coloration has lagged behind that of other groups, such as birds, because limited data exist on the color of extinct mammals known only from fossils, and no such attempt has been made for Mesozoic mammaliaforms (*9*).

Reconstructing the colors of fossil organisms was once thought to be impossible. However, the discovery that melanosomes, the melanin-containing organelles that produce colors in vertebrate integument, can be preserved in fossils as three-dimensional (3D) molds or imprints has revolutionized our understanding of integumentary coloration in deep time (*10*). Reconstruction of the colors of dinosaurs as far back as the Jurassic has elucidated the function and evolution of early feathers (*11*, *12*). The same is not true for mammal pelage, even though exquisite fossils with fur preservation were discovered more than a decade ago (*13*, *14*).

As in other vertebrates, mammalian melanosomes contain two chemical varieties of melanin: eumelanin, producing blacks and browns, and pheomelanin, producing yellows and reds (*15*). Colors of hair are produced by light absorption by a mixture of these two forms and have been associated with the morphology of the melanosomes themselves (*16*). Comparison of fossil and extant melanosomes can therefore enable reconstruction of fossil colors and, when coupled with broader analysis across the specimen, color patterns (*17*). We collected data on melanosome morphology (using scanning electron microscopy) and color (using microspectrophotometry) from hairs of 116 extant mammal species (n = 2615 melanosomes), including representatives of most clades in crown Mammalia, and produced a model that accurately predicts color from morphology. Whereas previous reconstructions have relied on binary, subjective color categories (*17*), we used spectrophotometric data to more precisely and objectively describe the spectrum of colors. We then applied this model to fossilized melanosomes in six phylogenetically and ecologically diverse taxa of the Yanliao and Jehol biotas from northeastern China, thereby reconstructing the pelage coloration of Mesozoic mammaliaforms. A previously undescribed fossil, intensively sampled and with the most complete fur preservation, is diagnosed by its distinctive dental pattern as a new species of Euharamiyida (*18*), adding to the known diversity in the Late Jurassic terrestrial ecosystem.

[1]State Key Laboratory of Biogeology and Environmental Geology, Frontiers Science Center for Deep-time Digital Earth, China University of Geosciences, Beijing, Beijing, China. [2]Evolutionary Ecology Group, Naturalis Biodiversity Center, Leiden, Netherlands. [3]Evolution and Optics of Nanostructures Group, Department of Biology, University of Ghent, Ghent, Belgium. [4]College of Earth Science and Engineering, Shandong University of Science and Technology, Qingdao, China. [5]Paleontological Institute, Shenyang Normal University, Shenyang, China. [6]Jackson School of Geosciences, University of Texas at Austin, Austin, TX, USA. [7]School of Biological Sciences, University of Bristol, Bristol, UK.
*Corresponding author. Email: liquanguo@cugb.edu.cn (Q.L.); matthew.shawkey@ugent.be (M.D.S.)

Systematic paleontology

Mammaliaformes Rowe, 1988 (*19*)
Euharamiyida Bi *et al.*, 2014 (*18*)
Arboroharamiyidae Zheng *et al.*, 2013 (*20*)
Arboroharamiya fuscus sp. nov.

Etymology. *fuscus* (Latin): dark, swarthy, dusky. The specific name *fuscus* refers to the dark coloration of pelage as reconstructed in this research.

Holotype. The holotype (CUGB-P1901, China University of Geosciences, Beijing, China) represents a partial skeleton exposed in ventral view (Fig. 1). The skull is partly preserved, teeth are dislocated and clustered around the skull, distal limbs and most of the phalanges are well preserved, and vertebrae (except caudal vertebrae) and integumentary tissues (including patagium for gilding) are preserved as impressions.

Locality and age. The specimen was collected from the Tiaojishan Formation at Nanshimen village, Gangou Township, Qinglong County, Hebei Province, China. The age of the strata is 158.58 million years within Oxfordian, Late Jurassic (*21*).

Diagnosis. Medium-sized euharamiyidan with a body mass estimated at 156 g. Dental formula presumed as I1-C0-P2-M2/i1-c0-p1-m2 (I, incisor; C, canine; P, premolar; M, molar; capital, upper teeth; lowercase, lower teeth) (Fig. 1). Similar to *Arboroharamiya jenkinsi* (*20*) but differing from other euharamiyidans in having larger teeth, P4 (ultimate upper premolar) being transversely wider than mesiodistally long, p4 (ultimate lower premolar) having simple distal heel with four minor cuspules distally, and molars bearing more cusps. Differs from *A. jenkinsi* in having M1 (first upper molar) subrhomboidal with longer mesial cusped ridge, m1 (first lower molar) narrower and with more cusps on both lingual and buccal rows; differs from *A. allinhopsoni* (*22*) in having four minor cuspules distally on the distal heel of p4 and more cusps on molars; differs from *Xianshou* (*18*) and *Vilevolodon* (*23*) in having larger tooth size and more cusps on cheek teeth. Further differs from *Mirusodens* (*24*), kermackodontids *Kermackodon* (*25*), and *Butlerodon* (*26*) in lacking heart-shaped P4, lacking secondary cusp row between the two primary cusp rows on upper molars, and lacking serrations on the hypertrophic a1 of p4. Further differs from shenshouids *Shenshou* (*18*) and *Qishou* (*27*) in lacking p4 submolariform with two cusp rows on the distal heel and having more cusps on cheek teeth with hypertrophic A1/a1; differs from *Maiopatagium* (*28*) in having enamel ridges and more conical cusps on cheek teeth with central basin closed mesially and distally. Further comparison and description of *A. fuscus* are included in the supplementary materials.

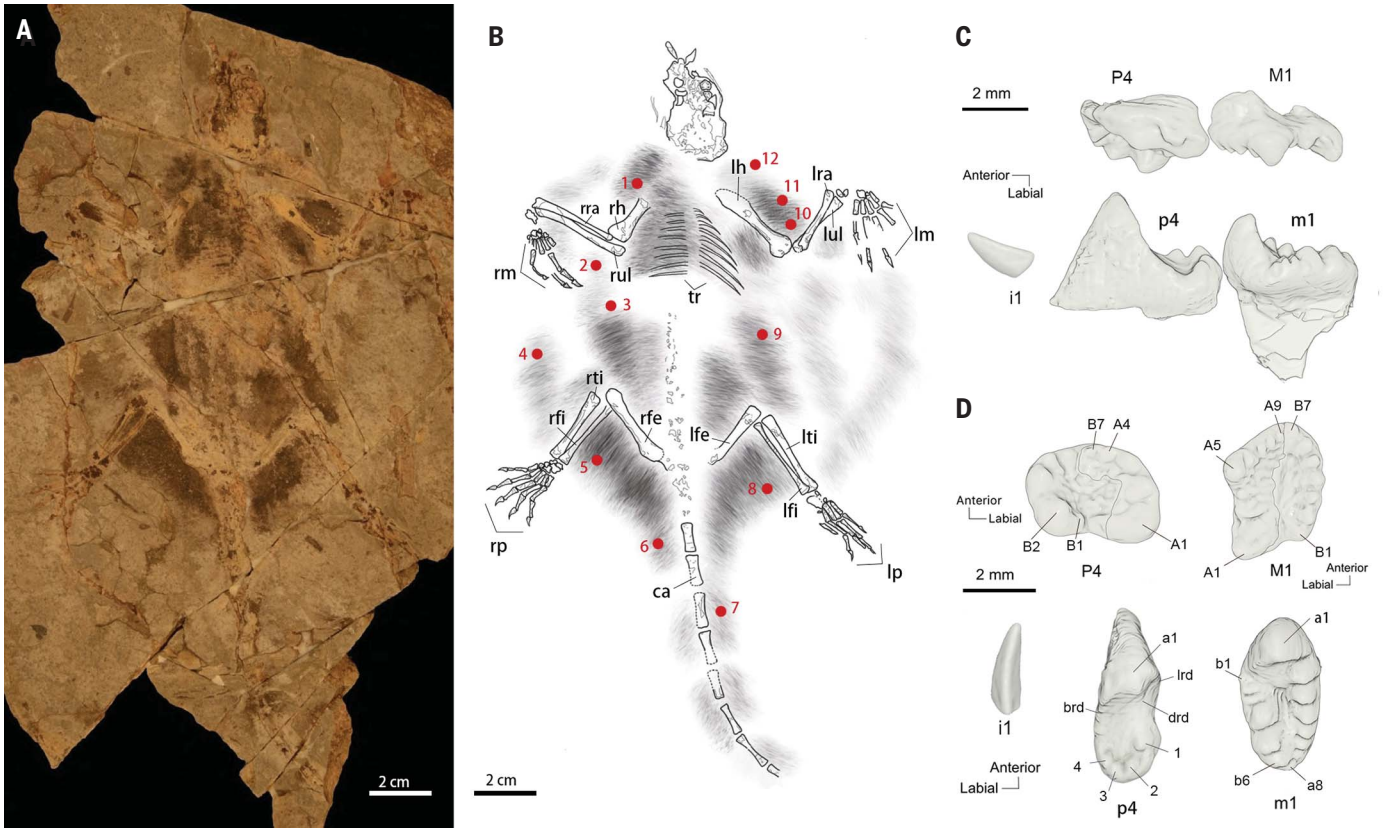

Fig. 1. The holotype specimen and teeth of *A. fuscus*. (**A**) The holotype specimen of *A. fuscus* (CUGB-P1901). (**B**) Line drawing of *A. fuscus*. Red dots represent sample locations for melanosome analyses. ca, caudal vertebrae; lfe, left femur; lfi, left fibula; lh, left humerus; lra, left radius; lm, left manus; lp, left pes; lti, left tibia; lul, left ulna; rfe, right femur; rfi, right fibula; rh, right humerus; rm, right manus; rp, right pes; rra, right radius; rti, right tibia; rul, right ulna; tr, thoracic ribs. (**C**) Upper and lower teeth in buccal view. P4, ultimate upper premolar; M1, first upper molar; i1, lower incisor; p4, ultimate lower premolar; m1, first lower molar. All teeth are from left dentition except M1, which is mirrored from the right first upper molar. (**D**) Occlusal views of teeth. All teeth are from left dentition except M1. The cusp tips on the buccal half of P4 and the lingual half of M1 were incomplete; cusp tips were reconstructed on the basis of preserved dentin and the outline of the tooth crown. brd, buccal ridge; drd, distal ridge; lrd, lingual ridge. Detailed description is included in the supplementary materials.

Integumentary impressions are preserved in the holotype specimen of *A. fuscus*, distributed as deep colored patches around the limb bones, torso, and caudal vertebrae (Fig. 1, A and B). Well-arrayed hairs are distinguishable in the matrix (Fig. 2, D and E, and fig. S2); these are thicker around the body and thinner in the outer area. There is no clear membrane edge preserved, but the extension of fine hair impressions in the area spanning between the wrists and ankles, along with thick hair impressions in the caudal area, suggests the location of the plagiopatagia and uropatagia (Fig. 2, C to E). X-ray fluorescence imaging (XRF) shows Ca and Cu enrichment correlated to hair impressions (Fig. 2C and fig. S4). Further examination under the scanning electron microscope revealed dense fossil melanosomes preserved both in 3D and in impression (Fig. 2, F and G, and fig. S3).

In addition to *A. fuscus*, we analyzed melanosomes of five other Mesozoic fossils preserved with integumentary impressions from the Yanliao and Jehol biotas of northeastern China (Fig. 2A and fig. S1; see supplementary materials, supplementary text section E). Three of the fossils [*A. fuscus*, *Megaconus mammaliaformis* (PMOL-AM00007), and *Vilevolodon diplomylos* (SDUST-V0010)] are placed in "Haramiyida," a taxon including the earliest gliders (*29*). Two fossils (SDUST-V0006 and SDUST-V0007) are assigned to Docodonta, a clade with species assessed to occupy diverse niches (e.g., fossorial, arboreal, or swimming) (*13*, *30*, *31*). The last fossil (SDUST-V0008) from the Lower Cretaceous is eutherian, placed in crown Mammalia. The phalangeal proportions and skeletal characteristics of the six fossils suggest that they belonged to distinct ecomorphotypes (Fig. 2B and fig. S5; supplementary materials, supplementary text section F). *A. fuscus* and *V. diplomylos* have patagia and prehensile claws, indicating an arboreal lifestyle and gliding ability. *M. mammaliaformis* and docodontan SDUST-V0006 are terrestrial and ground-living, whereas docodontan SDUST-V0007 shows heavy molar abrasion and thick bone walls, suggesting a ground-living habitat with fossorial ecology. Eutherian SDUST-V0008 has a pedal phalangeal index close to that of *Eomaia scansoria* (*32*), suggesting a scansorial or arboreal ecology (*32*, *33*). Among analyzed fossils, *M. mammaliaformis* (PMOL-AM00007), from the Middle Jurassic Tiaojishan Formation, is one of the oldest fossils reported with fur impression surrounding its body (*14*). Close examination shows that the fur of *M. mammaliaformis* was differentiated into thick guard hair and thinner underfur (*14*), but four other fossils from the Upper Jurassic (*A. fuscus*, *V. diplomylos*, SDUST-V0006, and SDUST-V0007) show no differences in hair diameter, with all hairs measuring between 0.02 and 0.04 mm (fig. S2). Although the hair impressions in eutherian SDUST-V0008 are scarce, a few of its distinguishable hairs also measure between 0.02 and 0.04 mm (fig. S2). Samples from hair impressions in all fossils show preservation of melanosomes (fig. S3).

With precautions to rule out influences of nonintegumentary tissues and shrinkage during diagenesis (see supplementary materials), we measured the geometry of fossil melanosomes

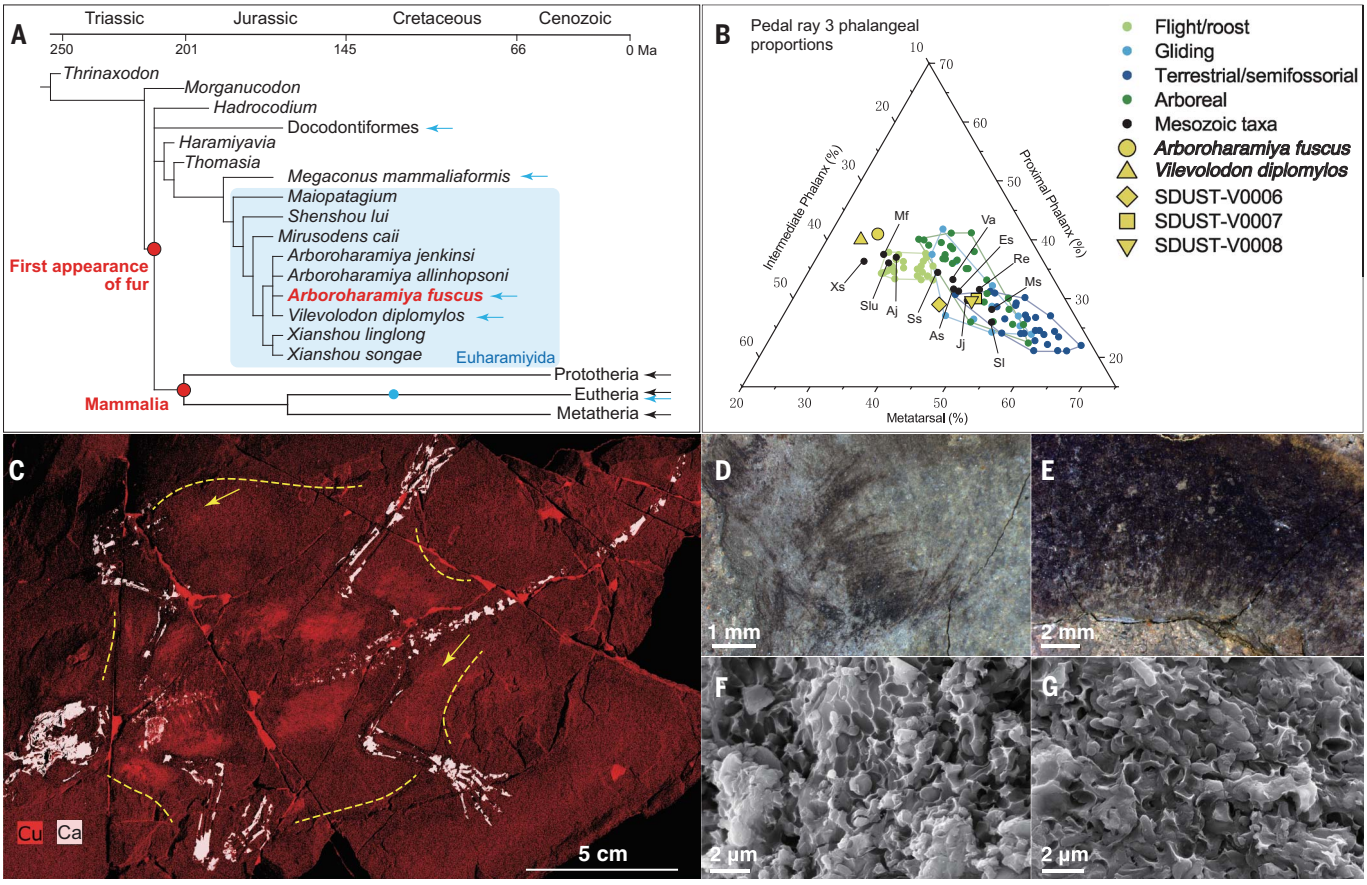

Fig. 2. Phylogenetic position of *A. fuscus*, phalangeal proportion analysis of five fossils, the Ca and Cu distribution, and hair and melanosome preservation in *A. fuscus*. (**A**) Phylogenetic position of *A. fuscus* in Euharamiyida (blue shaded rectangle); large-scale phylogeny tree is adopted from (*50*). Blue arrows, investigated fossils or the clade; black arrows, investigated extant mammalian clades; blue dot, the chronological position of SDUST-V0008. (**B**) Pedal ray 3 phalangeal proportion analysis of five fossils. Aj, *Arboroharamiya jenkinsi*; As, *Agilodocodon scansorius*; Es, *Eomaia scansoria*; Jj, *Jeholodens jenkinsi*; Mf, *Maiopatagium furculiferum*; Ms, *Maotherium sinensis*; Re, *Rugosodon eurasiaticus*; Slu, *Shenshou lui*; Sl, *Sinobaatar lingyuanensis*; Ss, *Sinodelphys szalayi*; Va, *Volaticotherium antiquus*; Xs, *Xianshou songae*. (**C**) Calcium distribution in *A. fuscus* is correlated with skeleton, and copper distribution is correlated with hair impressions. Dashed yellow lines represent the extension of patagium, and the two yellow arrows indicate magnified areas corresponding to (D) and (E). (**D**) Hair impressions preserved in the marginal area of the left plagiopatagia. (**E**) Dense hair impressions preserved in the caudal area. (**F**) Melanosomes in *A. fuscus* preserved as impressions. (**G**) Melanosomes in *A. fuscus* preserved as 3D molds.

in the six fossils, which exhibits high consistency both between and within fossil specimens and falls within the range of extant mammal melanosome measurements (Fig. 3). Extant mammal melanosomes are diverse in size and shape. Length varies within a range of ~1800 nm (346 to 2129 nm), and width varies within ~700 nm (219 to 921 nm). Thus, their aspect ratios range from 1.01 to 4.78 (i.e., almost spherical to highly tubular). By contrast, fossil melanosome geometries are confined to the upper end of extant melanosome size range, with lengths and widths varying by only ~500 and ~400 nm, respectively (Fig. 3), and all approximate an oval shape. Extreme melanosome shapes (either extremely round or elongated) as seen in extant mammals were not recovered from any of the fossils. Together, these data suggest that ancestral hair melanosomes are low-aspect-ratio (length/width < 2) with limited diversity, which is possibly linked with lower basal metabolic rates (fig. S7) (*34*). Our MCMCglmm analysis revealed a direct correlation between melanosome shape and hair color in extant mammals: Colorfulness (as measured by the first principal component of microspectrophotometric data) is negatively correlated with increasing length at a given width ($P < 0.005$) and positively correlated with width ($P < 0.005$) of melanosomes. That is, melanosomes of brightly colored hairs (such as red and orange) are more spherical, whereas melanosomes of dull-colored hairs (black, brown) are more elongated in shape. Furthermore, melanosome density, but not morphology, was significantly associated with the second principal component of color, which differentiates reds from yellows, suggesting higher melanosome densities in redder hairs than in less red hairs ($P = 0.005$). However, the melanosome density of fossil hair is not measurable, owing to the mixing of melanosomes from multiple hairs during fossilization. Surprisingly, no other variable, such as hair thickness or melanosome size variance, predicted coloration as they do in birds (see materials and methods), and microspectrophotometric data show that most individual mammalian hairs are brownish (even those perceived as black) and that true black or gray hairs are rare (fig. S6).

We reconstructed reflectance curves of fossil hairs for the assessed six taxa on the basis of the geometry of their melanosomes. All measurements from all sample locations on all fossils had predicted principal component 1 values corresponding to low reflectance and unsaturated coloration (Fig. 3 and table S5). XRF results of the fossils showed no evidence of Zn associated with pheomelanin (*35*) but high concentration of Cu associated with eumelanin in the integumentary impressions

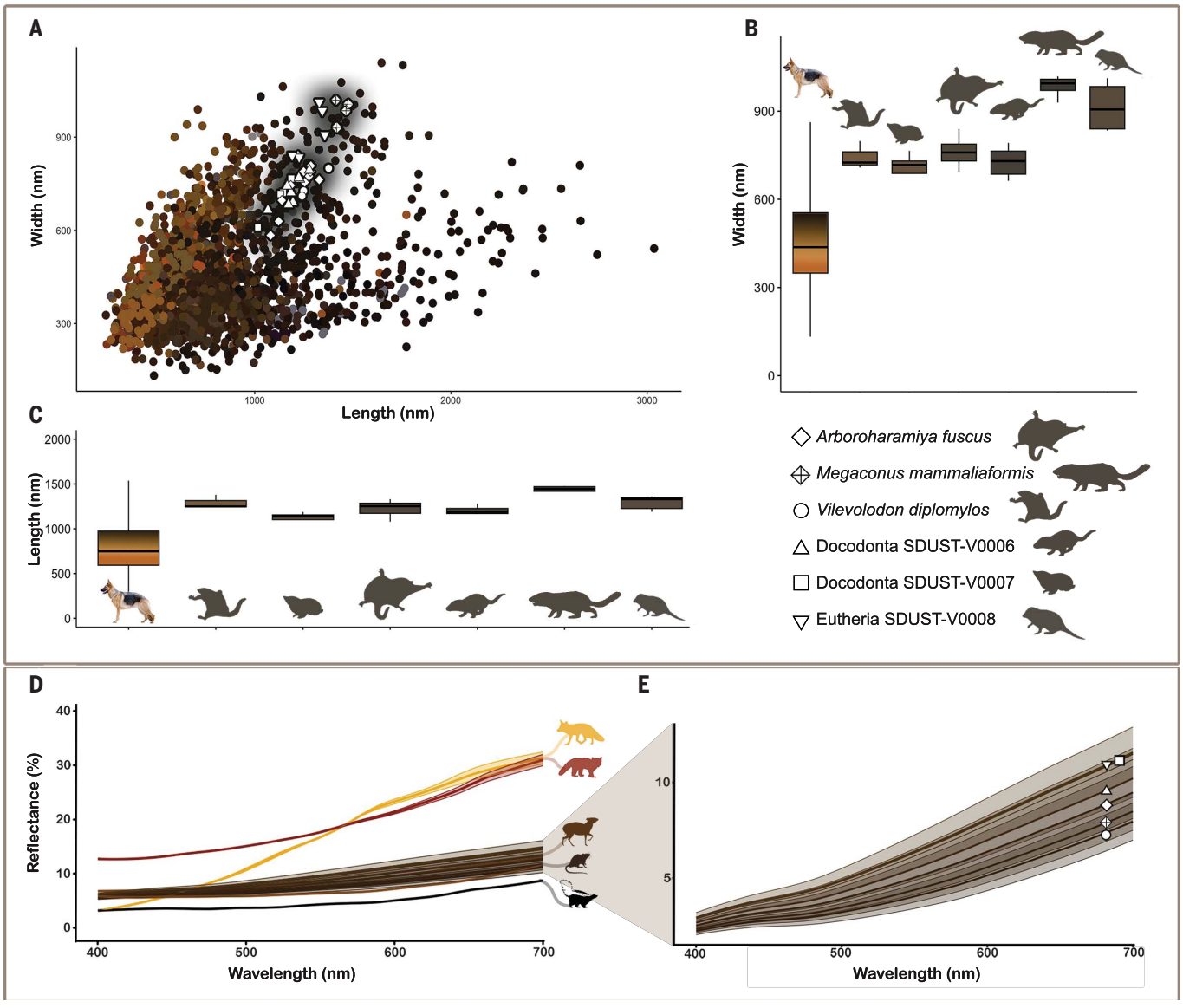

Fig. 3. Melanosome diversity and pelage coloration across extant mammals and Mesozoic mammaliaforms. (**A**) Scatterplot of individual melanosome measurements from 116 extant mammals and six fossils; dot color shows RGB values derived from spectral curves measured at specific hair locations. Extant hair melanosomes, *n* = 2615; *A. fuscus*, *n* = 760; *M. mammaliaformis*, *n* = 103; *V. diplomylos*, *n* = 395; docodontan SDUST-V0006, *n* = 289; docodontan SDUST-V0007, *n* = 407; eutherian SDUST-V0008, *n* = 205. (**B**) Width variation of melanosomes. (**C**) Length variation of melanosomes. (**D**) Measured reflectance spectra of selected extant mammals [*Vulpes vulpes* (orange), *Ailurus fulgens* (red), *Cephalophus dorsalis* (brown), *Pelomys fallax* (darker brown), and *Mephitis mephitis* (black)] and predicted reflectance curves for six Mesozoic mammaliaforms (browns), highlighting their constrained brown coloration and minimal variation. (**E**) Detailed view of the predicted reflectance curves for the six Mesozoic mammaliaforms.

(Fig. 2C and fig. S4) (*36*), supporting a dark coloration dominated by eumelanin. Together, these data indicate that the assessed six Mesozoic mammaliaforms had uniformly dark brown coloration with minor differences (Figs. 3 and 4).

Reconstructing the paleocolors of the six fossils provides physical evidence that pelage coloration in Mesozoic mammaliaforms was limited in diversity and darkly colored. The consistency in melanosome geometry of fossils suggests that, despite distinct variation in phylogeny and ecology, the melanin color system in Mesozoic mammaliaforms was largely invariant. This contrasts with the high diversity of melanosomes in feathered dinosaurs, early birds, and pterosaurs (*34*, *37*, *38*), indicating a different and unique evolutionary pattern of mammaliaform melanin color system after the sauropsid-synapsid split.

Samples taken from different integumentary locations of each fossil resulted in uniformly dark brown color, with no evidence of color patterns such as striping, spots, or countershading as seen in extant mammals, indicating that color patterns on the pelage might be a derived trait. Although the sex of fossils is difficult to determine, the highly confined reconstruction results suggest the absence of sexual dichromatism. The pelage coloration scheme in Mesozoic mammaliaforms was therefore unlikely for recognition or sexual display purposes but mostly for thermoregulation, for enhancing tactical sensory perception (*39*), for abrasion resistance, and for crypsis.

Most small Mesozoic mammaliaforms were likely nocturnal, as suggested by ancestral reconstruction of eye shape of extant mammals

(*40*, *41*) and phylogenetic inference of the genes involved in color perception and phototransduction (*42*). The compensatory sensory functions result from a combination of enhanced olfactory function, enhanced hearing by changes in the inner ear, and tactile sensation from fur (*39*, *43*). A nocturnal lifestyle may have enabled these species to avoid predation by diurnal carnivores and, furthermore, may have helped them to survive mass extinction (*44*). Our reconstruction results support the hypothesis that nocturnality might be ubiquitous in Mesozoic mammaliaforms, as dark-colored, uniformly dull pelage [which is mostly seen in nocturnal extant mammals (*4*)] is present in species occupying very different ecological niches. Additionally, highly melanized hairs could also be advantageous for thermoregulation and mechanical strength (*45*, *46*). Melanization increases heating speeds of materials (*45*), and darker hairs could help small mammaliaforms to reduce heat loss through insulation. Melanized materials are also stronger and abrasion-resistant (*46*), potentially enabling hairs to withstand wear and provide protection for the skin.

CREDIT: C. ZHAO

Fig. 4. Artistic reconstruction of pelage coloration of five Jurassic mammaliaforms. (Top to bottom) *A. fuscus* (CUGB-P1901), *V. diplomylos* (SDUST-V0010), *M. mammaliaformis* (PMOL-AM00007), and docodontans SDUST-V0006 and SDUST-V0007. The green eyes of *A. fuscus* are an artistic license of the tapetum lucidum, an intraocular reflecting structure that enhances visual sensitivity, indicating nocturnality. Eutherian SDUST-V0008 from the Lower Cretaceous is not included in this artistic reconstruction.

Extant mammals that inhabit ecological niches similar to the six fossils, such as fossorial moles (*Scalopus aquaticus*), mice and rats (*Lemniscomys griselda*, *Pelomys fallax*), and nocturnal bats (*Myotis myotis*, *Vespertilio murinus*), show a similar, very limited, color palette with mostly dark gray or brown colorations. However, diurnal or crepuscular species such as the Indian giant squirrel (*Ratufa indica*), red panda (*Ailurus fulgens*), and yellow-throated marten (*Martes flavigula*) exhibit vibrant purples, reds, and yellows, respectively. Daytime activity patterns may have enhanced the significance of sexual selection and intraspecific visual communication for the evolution of color and color patterns in extant groups. Melanosome diversity is also linked to the melanocortin system that affects not only melanin production but also numerous physiological and behavioral traits such as metabolic rate and appetite (*47*). Shifts in this system toward, for example, higher metabolic rates may have also led to the rapid evolution of melanosome shape within crown mammals (*48*). In any case, these changes of color employment through evolution likely developed under different pressures than for camouflage alone. After the Cretaceous-Paleogene event, mammals rapidly diversified into vacant niches previously occupied by dinosaurs (*49*), which could have simultaneously propelled the rapid radiation and diversification of pelage color strategies in new and diverse environments.

REFERENCES AND NOTES

1. I. C. Cuthill *et al.*, *Science* **357**, eaan0221 (2017).
2. D. Stuart-Fox, E. Newton, S. Clusella-Trullas, *Philos. Trans. R. Soc. Lond. Ser. B* **372**, 20160345 (2017).
3. N. Howell *et al.*, *Evolution* **75**, 2480–2493 (2021).
4. T. Caro, *Semin. Cell Dev. Biol.* **24**, 542–552 (2013).
5. C. R. Cooney *et al.*, *Nat. Commun.* **10**, 1773 (2019).
6. A. Roy, M. Pittman, E. T. Saitta, T. G. Kaye, X. Xu, *Biol. Rev. Camb. Philos. Soc.* **95**, 22–50 (2020).
7. H. K. Snyder *et al.*, *Biol. Lett.* **8**, 393–396 (2012).
8. T. Caro, *Trends Ecol. Evol.* **32**, 23–30 (2017).
9. M. E. McNamara *et al.*, *Trends Ecol. Evol.* **36**, 430–443 (2021).
10. J. Vinther, D. E. Briggs, R. O. Prum, V. Saranathan, *Biol. Lett.* **4**, 522–525 (2008).

11. Q. Li *et al*., *Science* **327**, 1369–1372 (2010).
12. D. Hu *et al*., *Nat. Commun.* **9**, 217 (2018).
13. Q. Ji, Z.-X. Luo, C.-X. Yuan, A. R. Tabrum, *Science* **311**, 1123–1127 (2006).
14. C.-F. Zhou, S. Wu, T. Martin, Z.-X. Luo, *Nature* **500**, 163–167 (2013).
15. L. D'Alba, M. D. Shawkey, *Physiol. Rev.* **99**, 1–19 (2019).
16. D. Grabolus, P. Wacławik, M. Zatoń-Dobrowolska, *Can. J. Anim. Sci.* **100**, 418–425 (2020).
17. J. Vinther, *Annu. Rev. Earth Planet. Sci.* **48**, 345–375 (2020).
18. S. Bi, Y. Wang, J. Guan, X. Sheng, J. Meng, *Nature* **514**, 579–584 (2014).
19. T. Rowe, *J. Vertebr. Paleontol.* **8**, 241–264 (1988).
20. X. Zheng, S. Bi, X. Wang, J. Meng, *Nature* **500**, 199–202 (2013).
21. Z. Yu *et al*., *Earth Planet. Sci. Lett.* **617**, 118246 (2023).
22. G. Han, F. Mao, S. Bi, Y. Wang, J. Meng, *Nature* **551**, 451–456 (2017).
23. Z.-X. Luo *et al*., *Nature* **548**, 326–329 (2017).
24. F. Mao, Z. Li, J. J. Hooker, J. Meng, *Zool. J. Linn. Soc.* **199**, 832–859 (2023).
25. P. M. Butler, J. J. Hooker, *Acta Palaeontol. Pol.* **50**, 185–207 (2005).
26. F. Mao, P. Brewer, J. J. Hooker, J. Meng, *J. Syst. Palaeontology* **20**, 1–37 (2022).
27. F.-Y. Mao, J. Meng, *Zool. J. Linn. Soc.* **186**, 529–552 (2019).
28. Q.-J. Meng *et al*., *Nature* **548**, 291–296 (2017).
29. D. M. Grossnickle *et al*., *Evolution* **74**, 2662–2680 (2020).
30. Q.-J. Meng *et al*., *Science* **347**, 764–768 (2015).
31. Z.-X. Luo *et al*., *Science* **347**, 760–764 (2015).
32. Q. Ji *et al*., *Nature* **416**, 816–822 (2002).
33. M. Chen, G. P. Wilson, *Paleobiology* **41**, 280–312 (2015).
34. Q. Li *et al*., *Nature* **507**, 350–353 (2014).
35. P. L. Manning *et al*., *Nat. Commun.* **10**, 2250 (2019).
36. R. A. Wogelius *et al*., *Science* **333**, 1622–1626 (2011).
37. K. K. Nordén *et al*., *Evolution* **73**, 15–27 (2019).
38. A. Cincotta *et al*., *Nature* **604**, 684–688 (2022).
39. T. B. Rowe, T. E. Macrini, Z.-X. Luo, *Science* **332**, 955–957 (2011).
40. M. P. Gerkema, W. I. L. Davies, R. G. Foster, M. Menaker, R. A. Hut, *Proc. Biol. Sci.* **280**, 20130508 (2013).
41. C. P. Heesy, M. I. Hall, *Brain Behav. Evol.* **75**, 195–203 (2010).
42. Y. Wu, H. Wang, E. A. Hadly, *Sci. Rep.* **7**, 46542 (2017).
43. T. B. Rowe, G. M. Shepherd, *J. Comp. Neurol.* **524**, 471–495 (2016).
44. E. Pennisi, *Science* **382**, 865–866 (2023).
45. M. D. Shawkey, A. M. Estes, L. M. Siefferman, G. E. Hill, *Proc. Biol. Sci.* **270**, 1455–1460 (2003).
46. R. H. C. Bonser, *Condor* **97**, 590–591 (1995).
47. A. L. Ducrest, L. Keller, A. Roulin, *Trends Ecol. Evol.* **23**, 502–510 (2008).
48. C. M. Eliason, J. A. Clarke, *Proc. Biol. Sci.* **285**, 20182014 (2018).
49. R. Maor, T. Dayan, H. Ferguson-Gow, K. E. Jones, *Nat. Ecol. Evol.* **1**, 1889–1895 (2017).
50. F. Mao *et al*., *Nature* **628**, 569–575 (2024).

ACKNOWLEDGMENTS

We thank A. Dong and C. Cao for CT scanning of the specimens; J. Yang and M. Yang for XRF scanning of the specimens; D. J. Tang and J. Hu for assisting with scanning electron microscopy analysis of the specimens; and C. Zhao for creating the artistic reconstruction image (Fig. 4). **Funding:** National Natural Science Foundation of China 42161134003 (Q.L., C.-F.Z., R.L.) ; National Natural Science Foundation of China 41872019 (Q.L., R.L.); Fundamental Research Funds for the Central Universities for the Frontiers Science Center for Deep-time Digital Earth, China University of Geosciences (Beijing) 2652023001 (Q.L., R.L.); Chinese "111" project B20011 (Q.L.); Taishan Scholar Program of Shandong Province tstp20240514 (C.-F.Z.); Flemish Research Funds FWO G0E8322N and G0A7921N (M.D.S., L.D.); Human Frontiers Science Program RGP0047 (M.D.S.); Air Force Office of Scientific Research FA9550-18-1-0477, FA9550-23-1-0622, and FA8655-23-2-7041 (M.D.S.). **Author contributions:** Conceptualization: L.D., J.V., J.A.C., Q.L., M.D.S.; Data curation: R.L., L.D., G.D., J.L.D., C.-F.Z., Q.L., M.D.S.; Funding acquisition: L.D., C.-F.Z., Q.L., M.D.S.; Project administration: R.L., G.D., J.L.D.; Supervision: L.D., C.-F.Z., Q.L., M.D.S.; Visualization: R.L., L.D., G.D.; Writing – original draft: R.L., G.D., J.L.D.; Writing – review & editing: R.L., L.D., G.D., J.L.D., C.-F.Z., J.A.C., J.V., Q.L., M.D.S. **Competing interests:** The authors declare that they have no competing interests. **Data and materials availability:** The fossil specimen CUGB-P1901 is accessioned at the University of Geosciences, Beijing (CUGB), China. The fossil specimens SDUST-V0006, SDUST-V0007, SDUST-V0008, and SDUST-V0010 are accessioned at Shandong University of Science and Technology (SDUST), Qingdao, China. The fossil specimen PMOL-AM00007 is accessioned at the Paleontological Museum of Liaoning (PMOL) at Shenyang Normal University, Shenyang, China. Detailed information on the specimens is listed in table S7. All fossil specimens are accessible to researchers. All data and phylogenetic datasets are provided in the supplementary materials.

SUPPLEMENTARY MATERIALS

science.org/doi/10.1126/science.ads9734
Materials and Methods
Supplementary Text
Figs. S1 to S7
Tables S1 to S7
References (*51–98*)
MDAR Reproducibility Checklist

Submitted 5 September 2024; accepted 28 January 2025
10.1126/science.ads9734